Title:

Comparative study on the efficacy and exposure of molecular target agents in non-small cell lung cancer PDX models with driver genetic alterations

Author:

Hitomi Jo[1,2], Shigehiro Yagishita[1], Yoshiharu Hayashi[1, 3, 4], Shoraku Ryu[1], Mikiko Suzuki[1, 3], Shinji Kohsaka[5], Toshihide Ueno[5], Yuji Matsumoto[6], Hidehito Horinouchi[7], Yuichiro Ohe[7], Shun-ichi Watanabe[8], Noriko Motoi[9], Yasushi Yatabe[9], Hiroyuki Mano[5], Kazuhisa Takahashi[2], Akinobu Hamada[1, 3*].

Affiliation:

[1]Division of Molecular Pharmacology, National Cancer Center Research Institute, 5-1-1 Tsukiji, Chuo-ku, Tokyo, Japan.

[2]Department of Respiratory Medicine, Juntendo University Graduate School of Medicine, 3-1-3, Hongo, Bunkyo-ku, Tokyo, Japan.

[3]Department of Medical Oncology and Translational Research, Graduate School of Medical Sciences, Kumamoto University, 1-1-1 Honjyo, Chuo-ku, Kumamoto, Japan.

[4]Bioanalysis Research Department, CMIC Pharma Science Co., Ltd., 17-18 Nakahata-cho,Nishiwaki, Hyogo, Japan

[5]Division of Cellular Signaling, National Cancer Center Research Institute, 5-1-1 Tsukiji, Chuo-ku, Tokyo, Japan.

[6]Department of Endoscopy, Respiratory Endoscopy Division, National Cancer Center Hospital, 5-1-1 Tsukiji, Chuo-ku, Tokyo, Japan.

[7]Department Thoracic Oncology, National Cancer Center Hospital, 5-1-1 Tsukiji, Chuo-ku, Tokyo, Japan.

[8]Department Thoracic Surgery, National Cancer Center Hospital, 5-1-1 Tsukiji, Chuo-ku, Tokyo, Japan.

[9]Department of Diagnostic Pathology, National Cancer Center Hospital, 5-1-1 Tsukiji, Chuo-ku, Tokyo, Japan.

Running title:

Efficacy and exposure in PDX models and NSCLC patients

*Corresponding author:

Akinobu Hamada, PhD.

Division of Molecular Pharmacology, National Cancer Research Institute.

5-1-1, Tsukiji, Chuo-ku, Tokyo 104-0052, Japan.

+81-3-3542-2511

akhamad@ncc.go.jp

Conflicts of interest:

The authors declare no potential conflicts of interest related to this work.

Abstract (240 words)

Patient-derived xenografts (PDXs) can adequately reflect clinical drug efficacy. However, the methods for evaluating drug efficacy are not fully established.

We selected five non-small cell lung cancer (NSCLC) PDXs with genetic alterations from established PDXs and the corresponding molecular targeted therapy was administered orally for 21 consecutive days. Genetic analysis, measurement of drug concentrations in blood and tumors using liquid chromatography and tandem mass spectrometry, and analysis of drug distribution in tumors using matrix-assisted laser desorption/ionization mass spectrometry were performed.

Fifteen (20%) PDXs were established using samples collected from 76 NSCLC patients with genetic alterations. The genetic alterations observed in original patients were largely maintained in PDXs. We compared the drug efficacy in original patients and PDX models; the efficacies against certain PDXs correlated with the clinical effects, while those against the others did not. We determined blood and intratumor concentrations in the PDX model, but both concentrations were low, and no evident correlation with the drug efficacy could be observed. The intratumoral spatial distribution of the drugs was both homogeneous and heterogeneous for each drug, and the distribution was independent of the expression of the target protein.

The evaluation of drug efficacy in PDXs enabled partial reproduction of the therapeutic effect in original patients. A more detailed analysis of systemic and intratumoral pharmacokinetics may help clarify the mode of action of drugs. Further development of evaluation methods and indices to improve the prediction accuracy of clinical efficacy is warranted.

Introduction

The developmental success rate for anticancer drugs is very low, with only 5% of the drugs approved for clinical application even despite a good preclinical response (1,2). This is partly because traditional drug screening using cell lines is less predictive of clinical efficacy (3). In this context, the patient-derived xenograft (PDX) model, established by implanting a patient's tumor tissue directly into immune-deficient mice, has recently been considered as a possible solution. The PDX retains the original tumor's biological characteristics and heterogeneity as the tumor cells and its entire surrounding microenvironment are transplanted (4-6). Compared to cell lines or cell line xenograft models, PDXs better reflect the therapeutic effect with more than 80% similarity between clinical data and PDX responses in some instances (3,7,8).

Over the past two decades, the treatment landscape for non-small cell lung cancer (NSCLC) has changed dramatically owing to a better understanding of the disease biology and mechanisms of tumor progression (9). Specifically, the use of small-molecule tyrosine kinase inhibitors (TKIs) and immunotherapy has improved survival rates in NSCLC patients (10-12). The treatment strategy for lung adenocarcinoma is determined by gene profiling, such as epidermal growth factor receptor (EGFR) mutation, anaplastic lymphoma kinase (ALK) fusion, ROS proto-oncogene 1 (ROS1) fusion, and v-raf murine sarcoma viral oncogene homolog B1 (BRAF mutation) (13). It is indisputable that molecularly targeted therapies improve patient survival and quality of life and a more individualized treatment strategy is required (9,14). Treatment strategies for NSCLC patients should focus on the genetic alterations and the resistance mechanisms after drug administration (15). However, due to the diversity of these resistance mechanisms and the rarity of the disease, it is difficult to conduct prospective randomized clinical trials (16).

PDXs have been reported in NSCLC (17-22). A co-clinical trial generated PDXs in conjunction with clinical trials and reported the drug resistance mechanisms (23). In addition to their use in the exploration of drug resistance mechanisms and their application in drug efficacy evaluation, there exists a strong correlation between the treatment response in original patients and corresponding PDXs (18). The therapeutic strategies for lung cancer are increasingly fragmented based on genetic alterations and resistance mechanisms; however, PDX is expected to be useful for drug development, for overcoming drug resistance, and for reducing the lag in clinical trials by enabling the conduction of early proof-of-concept testing in preclinical studies.

PDX demonstrates substantial potential utility for studying drug efficacy; however, the most remarkable limitation is the lack of a defined methodology for studying drug efficacy in PDX to predict clinical efficacy. It is necessary to ascertain various factors such as the number of mice to be used, criteria for commencement of the study, evaluation method, drug dosage, and administration schedule. Additionally, the prediction of clinical efficacy as an endpoint must be evaluated; however, the criteria and

indicators for evaluating the prediction are not determined. In this context, we propose that drug concentration and drug distribution are important factors that will enable PDX utilization for testing drug efficacy in humans. Phase 1 studies in humans are conducted after evaluation in animal models such as mice, dogs, and monkeys in the clinical development of anticancer drugs. The only standard indicator evaluated in these studies is the drug concentration in blood. Therefore, the blood concentration may be deemed one of the evaluation indices for comparing the therapeutic effects between PDX and humans.

Many drugs, including anticancer drugs, exert their pharmacological effects in tissues, but not in plasma where the drug concentrations are usually measured. Plasma concentrations are not necessarily representative of the drug concentrations in the tissues. We previously reported the heterogeneous spatial distribution of anticancer drugs in several tumors, using matrix-assisted laser desorption/ionization mass spectrometry (MALDI-MSI) (24-27). The actual distribution and the concentration of drugs in the tumors are unclear, and it is often challenging to obtain human specimens after drug administration. The intratumor distribution of anticancer drugs is a potential evidence of the mode of action; therefore, a validated method to confirm whether drugs have reached the right target is an urgent need for drug development in oncology. PDX is considered an optimal platform for the simultaneous analysis of drug concentration and heterogeneous spatial distribution in tumors and the plasma drug concentration, because it preserves tumor heterogeneity and tissue structure in patients' tumors and enables repeated tumor sample collection at any instance after drug administration.

The aim of this study was to characterize the establishment of PDXs using NSCLC samples and to evaluate the utility of the PDX models in the original patients in terms of genetic alterations, protein expression, plasma drug concentration, and spatial distribution of the drug in tumor tissue (**Figure 1**). We have discussed and provided description of the optimal use of PDX to predict clinical efficacy.

Materials and Methods

Patient-derived xenograft model

PDX samples were provided by the National Cancer Center J-PDX library, Japan. The protocol was approved by the institutional review board (NCCRI: 2015-123), and all patients provided written informed consent. Lung cancer PDX models of cases with driver mutations were selected (**Figure 1A**). The study was performed according to the precepts established by the Helsinki Declaration; its design and conduct complied with all applicable regulations, guidance, and local policies. Animal experiments were performed in compliance with the Institute for Laboratory Animal Research guidelines, National Cancer Center Research Institute (T17-073 and T19-008). The first engrafted PDX established by transplanting the patient's original tumor was designated trans-generation 1 (TG1) and subsequently TG2 and TG3. In the present study, we used PDXs from TG3 to TG4.

Reagents

The following drugs used in this study were purchased from Selleck Biotech (Tokyo, Japan): brigatinib (S8229), lorlatinib (S7536), gefitinib (S1025), osimertinib (S7297), afatinib (S1011), poziotinib (S7358), crizotinib (S1068), and entrectinib (S7998). Trastuzumab deruxtecan (T-DXd) was kindly provided by Daiichi Sankyo (Tokyo, Japan).

Patients' characteristics and clinical information

Patients' characteristics, including age, sex, Eastern Cooperative Oncology Group (ECOG) performance status (PS), smoking history, and medical history, were collected. According to the Union for International Cancer Control classification for each tumor, tumor characteristics, including histology and tumor-node-metastasis (TNM) stage, were noted. Biomarker data, including gene analysis results of companion diagnostics and clinical sequencing, were collected from medical records. Prior treatment characteristics, including chemotherapy regimens, cycles of chemotherapy, and best response, were collected.

Animal experiments

Four-to-six-week-old female SCID-Beige mice (CB17.Cg-PrkdcscidLystbg-J/CrlCrlj, Charles River Laboratories Japan, Kanagawa, Japan) were purchased. Mice were housed in sterile filter-capped polycarbonate cages, maintained in a barrier facility under a 12-hour light/dark cycle, and provided sterilized food and water. All invasive procedures were performed by intraperitoneal administration of three types of mixed anesthesia (medetomidine hydrochloride, Meiji Seika Pharma, Tokyo, Japan; midazolam, Maruishi Pharmaceutical, Osaka, Japan; betorfal tartrate, Meiji Seika Pharma) or inhalation of isoflurane (Zoetis Japan, Tokyo, Japan) to reduce the pain of the experimental animals. After receiving TG2 or TG3 frozen PDX tumor samples, the tumors were thawed and implanted into both flanks of SCID-Beige mice under anesthesia. When the tumors grew, they were transplanted into the right flank of multiple mice and used for drug efficacy tests. Mouse body weight and tumor growth were assessed twice

weekly. Tumors were measured with a caliper, and tumor volumes were calculated using the formula: tumor volume (mm^3) = (tumor length (mm) × [tumor width $(mm)]^2$) / 2. When the tumor growth reached approximately 500–1000 mm^3, they were cut into 2 mm cubic and transplanted into multiple mice for drug efficacy testing.

When the implanted tumors grew to approximately 150–250 mm^3, grouping of the PDX mice was conducted using software calculations (EXSUS, CAC Croit, Tokyo, Japan) to minimize tumor volume differences between groups. Each PDX drug efficacy study consisted of three or more groups (4-10 mice per group): a control group and two or more drug treatment groups. The correspondence between the PDX and the drugs administered is shown in **Figure 1B**. T-DXd was administered intravenously *via* tail vein on day 0, and all other drugs including vehicle (normal saline) were administered orally once a day for 21 consecutive days. The dosage of each drug was set at an appropriate amount based on previous reports (28-32). All mice were euthanized due to cervical dislocation, and the blood and tumor tissue were collected at 24 h after conduction of the last drug administration on day 21. Tumor samples were snap-frozen by liquid nitrogen after collection and stored at -80 °C until analysis. Blood samples were collected in EDTA-2K tubes, centrifuged (1200 × g for 10 min at 4 °C), and then the plasma was stored at -80 °C until analysis.

The antitumor effect was shown as %Growth (%Gr) by comparing the tumor growth increment in the control at day 0 and treatment groups at day 21.

ΔC = (Tumor volume of the control group at day 21) – (Tumor volume of the control group at day 0)

ΔT = (Tumor volume of treatment group at day 21) – (Tumor volume of treatment group at day 0)

%Gr = 100 x ($\Delta T / \Delta C$)

Histological and immunohistochemistry analysis

PDX tissues were fixed in 10% buffered formalin and then subjected to hematoxylin and eosin (H&E) staining, and a qualified pathologist confirmed NSCLC diagnoses and histopathological characteristics. Frozen tumor sections of xenografts were also stained with H&E after MSI analysis. For immunohistochemistry (IHC) staining of LC-001, LC-002, and LC-004, frozen sections were fixed in 10% buffered formalin for 10 min at 25 °C. Sections were then incubated with 0.3% H_2O_2 in methanol at 25 °C after washing with 1×TBS. Sections were incubated in serum-free protein block solution (X0909; Dako, Tokyo, Japan) for 15 min at 25 °C, followed by incubation with primary antibody overnight at 4 °C: ALK (D5F3) XP® Rabbit mAb (#3633, 1:500; Cell Signaling Technology, Danvers, MA, USA), ROS1 (D4D6) Rabbit mAb (#3287, 1:250; Cell Signaling Technology), or HER2 (4B5) (Roche, Bazel, Switzerland). After washing with 1×TBS, signal stain boost IHC detection reagent (#8114, anti-rabbit; Cell Signaling Technology) was added and incubated for 30 min at 25 °C. Sections were reacted with diaminobenzidine (#8059S; Cell Signaling Technology) and counterstained with hematoxylin. A BZ-X710 microscope (Keyence, Osaka, Japan) was used for histologic photography.

Nucleic acid extraction

Nucleic acids were extracted using pleural fluid (patient B and D) or FFPE samples (patient A and C) from patient tumors and fresh frozen tumors from PDX tumors. Genetic analysis was performed using patient tumors and PDX tumors of TG1, TG2, and TG3 in LC-001 to LC-003, patient tumors and PDX tumors of TG1 in LC-004, and patient tumors and PDX tumors of TG1 and TG2 in LC-005. DNA and RNA were extracted from FFPE samples using a GeneRead DNA FFPE Kit (Qiagen, Hilden, Germany) and an RNeasy FFPE Kit (Qiagen), and from pleural fluid and fresh frozen tumors using either a KingFisher Cell and Tissue DNA Kit (Thermo Fisher Scientific, Waltham, MA, USA) or a MagMAX mirVana Total RNA Isolation Kit (Thermo Fisher Scientific).

Whole-exome sequencing, including mutation calls, and copy number analysis

Whole-exome sequencing (WES) samples were prepared using a Twist Comprehensive Exome Kit (Twist Bioscience, San Francisco, CA, USA). Library concentration was measured by a Qubit 2.0 Fluorometer (Thermo Fisher Scientific). Library quality was considered sufficient if a single peak between 250–350 bp was detected by the Agilent 2200 TapeStation system (Thermo Fisher Scientific). Sequencing analysis was performed on an Illumina NovaSeq 6000 system (Illumina, San Diego, CA, USA). Paired-end WES reads were aligned to the combined human (hg38) and *Mus musculus* (mm10) reference genome using BWA (27). Both somatic synonymous and non-synonymous mutations were called using our in-house caller and two publicly available mutation callers: Genome Analysis Toolkit (https://gatk.broadinstitute.org/hc/en-us) MuTect2 and VarScan2 (http://varscan.sourceforge.net/). Mutations were discarded if any of the following criteria were met: the total read number was <20, the variant allele frequency in tumor samples was <0.05, the mutant read number in the germline control samples was >2, the mutation occurred in only one strand of the genome, or the variant was present in normal human genomes in either the 1000 Genomes Project dataset (https://www.internationalgenome.org/) or our in-house database. Gene mutations were annotated by SnpEff (https://pcingola.github.io/SnpEff/). The copy number status was analyzed using our in-house pipeline, which determines the log R ratio (LRR) as follows: (1) SNP positions in a homozygous state (variant allele frequency (VAF): ≤0.05 or ≥0.95) or heterozygous state (VAF: 0.4-0.6) in the genomes of respective normal samples were selected from the 1000 Genomes Project database; (2) normal and tumor read depths at the selected position were adjusted based on the GpC percentage of a 100-bp window flanking the position (33), (3) the LRR was calculated as the $\log_2(t_i/n_i)$, where n_i and t_i represent the normal and tumor-adjusted depths at position i, respectively; and (4) each representative LRR was determined by the median of a moving window (1 Mb) centered at position i. The LRRs of the copy numbers of alleles, the major allele, and the minor allele were determined for every region of the genome.

Transcriptome sequencing, expression analysis, and detection of fusion genes

Total RNA was treated with DNase I (Thermo Fisher Scientific) and subjected to poly (A)-RNA selection prior to cDNA synthesis. The library used for RNA-sequencing was prepared using a NEBNext

Ultra Directional RNA Library Prep Kit (NEB, Ipswich, MA, USA), following the manufacturer's protocol. Sequencing was conducted from bh ends of each cluster using a NovaSeq 6000 (Illumina). RNA-sequencing reads were aligned to the merged hg38 and mm10 reference genome using STAR (https://github.com/alexdobin/STAR) with the annotated human (release 31) and *Mus musculus* (release M24) GTF files distributed by GENCODE (https://www.gencodegenes.org/).

Pharmacokinetic analysis

LC-MS/MS was employed to measure the concentration of each drug (free fraction). For plasma preparation, briefly, 20 μL mouse plasma was mixed with 100 μL internal standard solutions in MeOH for protein precipitation. All samples were vortexed for 10 s and centrifuged at 12000 x *g* for 10 min at 4 °C. The supernatants were separated and applied for LC-MS/MS analysis. For tumor samples, three consecutive tumor sections, before and after the section for MSI, respectively, were collected in 2 polypropylene tubes. Tumor sections were homogenized in 50 μL methanol by vortex-mixing for 1 min. Then, the internal standard solution in MeOH was added and vortex-mixed for 10 s. After centrifuging at 12000 x *g* for 10 min, the supernatant was collected. A portion of the supernatant was applied for LC-MS/MS analysis, and the rest was used for protein quantification using a Qubit 2.0 Fluorometer (Qubit Protein Assay Kit, #Q33211, Thermo Fisher Scientific). The drug concentration in the tissue section was calculated by dividing drug quantity (measured by LC-MS/MS) by the protein amount in the corresponding tissue extract.

Instruments used for LC-MS/MS analysis were the Nexera X2 UHPLC system (Shimadzu, Kyoto, Japan) connected with a QTRAP5500 mass spectrometer (AB SCIEX, Framingham, MA, USA). The electrospray ionization interface in the positive mode was used to perform MS/MS. The multiple reaction monitoring (MRM) transitions for all compounds (**Supplementary Table 1A**), the LC conditions for separating (**Supplementary Table 1B**), and the optimized MS/MS parameters for each compound (**Supplementary Table 1C**) are presented. The developed methods were validated in terms of specificity, linearity, accuracy, and precision using blank mouse plasma spiked with standard solutions.

Mass spectrometry imaging

For quantification drug concentrations and imaging drug distributions in tumor tissues, the frozen tissues were successively sliced into 8-μm-thick slices at -20 °C with a cryomicrotome (Leica CM 1950; Leica Biosystems, Tokyo, Japan) and placed on the adhesive glass slides coated with an indium tin oxide (SI0100N; Matsunami Glass, Osaka, Japan). We used matrix-assisted laser desorption/ionization mass spectrometry imaging (MALDI-MSI) in this study because MALDI-MSI is the most widely used visualization technique in pharmacokinetic studies (24). α-CHCA was applied to the aforementioned section tissue surface at 250 °C for 8 min using a sublimation apparatus (SVC-700TMSG/7PS80; Sanyu Electron, Tokyo, Japan). Subsequently, 10 mg/mL α-CHCA in ultrapure water/acetonitrile/IPA/TFA = 60/30/10/0.1, v/v/v/v was sprayed stepwise onto the sections using a sprayer (PS270; GSI Creos, Tokyo, Japan) (24,27). MALDI-MSI analysis was performed in positive ionization mode using iMScope

(Shimadzu, Kyoto, Japan), which consisted of an optical microscope and an ion trap time-of-flight analyzer with an atmospheric pressure MALDI source consisting of a 335 nm Nd:YAG laser. The protonated molecules of drugs were fragmented by low energy collision-induced dissociation with Ar gas; the isolation width was 3 Da. Fragment patterns are illustrated in **Supplementary Figure 1**. One fragment ion each drug was selected, and that ion was used for imaging of drugs. The mass tolerance was 50 mDa. Selected ions and the setting values of laser power and collision energy are listed in **Supplementary Table 1D**. The laser was fired 200 shots at a repetition rate of 1000 Hz per spot; the pitch of the laser shot was 50 μm. Imaging data were obtained using Imaging MS Solution (ver. 1.20; Shimadzu) and analyzed using Imaging IMAGEREVEAL (ver. 1.12; Shimadzu). The chromatogram for each compound is shown in **Supplementary Table 2**.

Statistical analysis

All data were analyzed using GraphPad Prism ver. 8.3 (GraphPad software, San Diego, CA, USA) and SAS ver. 9.4 (SAS Institute, Cary, NC, USA). For drug testing, statistically significant differences between control and each group at day 21 were tested as follows: (1) Bartlett's test was used as a test for the equality of k variances; (2) If the k sampled populations had equal variances ($p > 0.05$ by Bartlett's test), Dunnett's multiple comparison test was performed; otherwise, Steel's test was used. $P < 0.05$ was considered statistically significant.

Data availability

The data generated in this study are publicly available in National Bioscience Database Center (NBDC) / the Japan Science and Technology Agency (JST) under the accession number JGAS000413.

Results

Establishment of lung cancer PDXs

From August 2018 to May 2020, a total of 245 lung cancer specimens were registered for J-PDX, 21 for small cell lung cancer (SCLC), and 224 for NSCLC (34). In total, 55 PDXs were established, including 8 SCLC PDXs and 47 NSCLC PDXs. Of these NSCLC PDXs, 15 PDXs reported genetic aberrations in the clinical information: 7 EGFR mutations, 5 ALK fusion, 1 ROS1 fusion, 1 RET fusion, and 1 HER2 amplification (**Figure 1A**). The overall establishment rate was 22%, and by histological subtype, SCLC accounted for 38% and NSCLC accounted for 21%. The establishment rate was 16% for adenocarcinoma and 35% for squamous cell carcinoma, and the establishment rate tended to be higher in chemotherapy-resistant specimens than in chemotherapy-naive specimens (**Supplementary Table 3A**). The establishment rate by genetic alteration is shown in **Supplementary Table 3B**. The establishment rate of EGFR mutation-positive cases was 16% (7/43) in all and 19% (7/36) in the TKI-resistant samples. In contrast, the establishment was not found in the TKI-naïve samples. The establishment rates of ALK fusion, ROS1 fusion, HER2 amplification, MET skipping, and RET fusion were 21% (5/24), 33% (1/3), 100% (1/1), 0% (0/1), and 25% (1/4), respectively. Overall, NSCLC with genetic aberrations tended to have a higher establishment rate in treatment-resistant specimens than in treatment-naïve specimens.

NSCLC PDXs with driver gene alteration

We used 5 of the 15 established NSCLC PDXs and tested their efficacy against TKIs and several unapproved drugs administered to patients. **Table 1** shows the clinical characteristics of the four patients, PDX sample origins, and collection points of tumors from patients and corresponding PDXs. The clinical driver gene for each patient is as follows: Patient A, ALK fusion; Patient B, EGFR exon 21 L858R mutation; Patient C, ROS1 fusion; and Patient D, HER2 amplification. Two PDXs, LC-001 and LC-002, were established by two longitudinal pleural fluid samples in patient A, and a single PDX was established in each of the other patients.

Gene analysis

To confirm changes in genetic alterations from passaging tumor grafts, we performed WES and RNA-sequencing of clinical samples and PDX tumors. The patient tumor samples used in the analysis, the time of collection, and its contrast to PDX tumors with representative genetic abnormalities are shown in **Table 1**. LC-001 sequencing analysis showed ALK fusions in TG1 and TG3 PDX tumors, but not in the patient tumor or TG2 PDX tumor, possibly due to the specimen collection site, quantity, or quality. LC-004 showed EZR-ROS1 fusion in PDX tumors. Although HER2 amplification was reported in the clinical sequence by Oncomine Comprehensive Assay v3 (Thermo Fisher Scientific) in LC-005, neither HER2 amplification nor gene mutation was observed in the patient tumors or PDX tumors in this study. On the other hand, HER2 immunostaining of PDX tumors consistently showed strong protein expression of HER2, and RNA-sequencing also showed high expression levels in both the patient and PDX tumors

(**Supplementary Figure 2**). Overall, the clinical driver genes were found to be largely maintained in PDX tumors. Somatic mutations with allele frequencies of 10% or higher and genes with copy number amplifications of 6 or higher in WES are shown in **Supplementary Tables 4 and 5**, respectively.

Histopathological comparison of PDX models by generation

We compared the histological findings from the original patient tumors and each passaged PDX tumor (TG1-3, **Figure 2**). Morphologically, in LC-005 PDX, the original and PDX tumors had similar morphology. In the other PDX tumors, some of the original tumor morphology was preserved, but there was a tendency for PDX tumors to be less differentiated histologically than the original tumors.

Patients and PDX models

We conducted an *in vivo* drug test using the five NSCLC PDXs with driver gene alterations. **Figure 3** shows the original patient's clinical course and the drug efficacy in the corresponding PDXs. The drugs selected were either TKIs administered to the original patient or administered after the PDX sample collection, and drugs with suggested efficacy against the respective gene alterations.

Patient A: EML4-ALK fusion

Patient A received first-line treatment for ALK-positive lung adenocarcinoma with alectinib, followed by various cytotoxic agents and ceritnib, and then lorlatinib was administered as fifth-line therapy (**Figure 3A**). LC-001 was established from the pleural effusion at the early stage of lorlatinib treatment, and LC-002 was established from the pleural effusion at the time of disease progression of lorlatinib. ELM4-ALK fusion was maintained in almost all PDX tumors. However, there was no secondary mutation in the ALK gene or other reported resistance mechanisms. The drug test was conducted using LC-001 and LC-002 with either lorlatinib, a clinically administered ALK inhibitor, or brigatinib, a novel ALK inhibitor not approved at the time. Both lorlatinib and brigatinib showed a constant efficacy in LC-001, but LC-002 showed a decreased sensitivity to brigatinib. Clinically, there was a rapid increase in pleural effusion within a short period of 2 weeks of lorlatinib administration, suggesting a discrepancy between the PDX results and the clinical response.

Patient B: EGFR ex21 L858R with EGFR and MET amplification

Patient B received gefitinib as the first-line treatment for EGFR mutation-positive lung adenocarcinoma with a short-term progression of 2.5 months and presented with negative results for the T790M mutation (**Figure 3B**). The patient was subsequently enrolled in a clinical trial and demonstrated an exacerbation at 6 months. After the second exacerbation, LC-003 was established from a bronchoscopic specimen and tested for efficacy with gefitinib, a clinically refractory drug, and osimertinib, a novel third-generation EGFR-TKI that had not been administered previously. Gene analysis of tumor tissue at diagnosis and PDX tumors showed that EGFR ex21 L858R was maintained at a constant allele frequency, whereas ex20 T790M was not found. On the other hand, copy number analysis showed EGFR

and MET amplification, suggesting that these amplifications resulted in EGFR-TKI resistance. *In vivo*, consistent with the clinical effect, no antitumor effect was observed with gefitinib treatment, whereas osimertinib showed some therapeutic effect.

Patient C: EZR-ROS1 fusion

Patient C received platinum combination therapy and an immune checkpoint inhibitor for lung adenocarcinoma, with ROS1 fusion identified during the course of the therapy **(Figure 3C)**. LC-004 was established from the pleural effusion before crizotinib administration. Patient C responded well to crizotinib, but an explained sudden death on the 20th day after initiation of crizotinib made it impossible to evaluate the treatment efficacy. The drug testing of the clinically administered crizotinib and the recently approved drug for ROS1 fusion, entrectinib, showed significant *in vivo* antitumor activity.

Patient D: HER2 amplification

Patient D had a HER2 amplification-positive lung adenocarcinoma treated with a platinum combination and immune checkpoint inhibitors (**Figure 3D**). LC-005 was established from a pleural effusion after second-line atezolizumab exacerbation. We conducted a drug testing using the pan-HER inhibitors afatinib and poziotinib and the anti-HER2 antibody-drug conjugate T-DXd, which recently showed dramatic efficacy against HER2-positive breast and gastric cancer (35,36). For pan-HER inhibitors, poziotinib showed a significant promising effect, whereas afatinib showed no antitumor effect. On the other hand, T-DXd showed significant tumor shrinkage in a dose-dependent manner.

Drug exposure and target delivery

For the eight TKIs tested in this study, we analyzed drug concentrations in plasma and tumor samples to explore the reasons for the discrepancy between the clinical and PDX models (**Table 2**). The 21-day dosing period in humans is the potential required duration for plasma concentrations to reach a steady-state phase; however, in the PDX model, the mouse plasma concentrations of the eight drugs administered were low for all drugs and below the lowest limit of quantitation (LLOQ, 2 ng/mL) for osimertinib, gefitinib, and afatinib. The tumor drug concentrations, which were normalized to protein amounts in tumor sections, tended to be higher than the plasma level for brigatinib, crizotinib, and entrectinib but below plasma concentration levels for the other drugs. These results suggest that it is difficult to infer the therapeutic relationship between antitumor activity in PDXs and clinical efficacy from the blood and intratumor drug concentrations.

Visualized drug distribution

Since LC-MS measurement is based on homogenized tumor tissue and greatly affected by blood adhesion, it cannot assess the drug's spatial distribution. Therefore, MSI was performed to assess intratumoral structures and spatial distribution of drugs. All eight TKIs used in this study were examined, and the three drugs, brigatinib, crizotinib, and entrectinib, were effectively analyzed. H&E staining, IHC for

each TKI target protein (ALK protein in brigatinib, ROS1 protein in crizotinib and entrectinib), and MSI are shown in **Figure 4A**. The intratumoral distribution of each drug was independent of the localization of the corresponding target protein. Comparison of the region of interest between the tumor and non-tumor sites showed a clear accumulation at tumor sites for brigatinib but no obvious difference by tissue structure for crizotinib and entrectinib (**Figure 4B, Supplementary Table 6**).

Discussion

  In this study, we focused on NSCLC PDXs with genetic alterations and explored the factors that influence the establishment rate of PDXs. We found that PDXs were more likely to be established in patients with a history of treatment with molecular targeted drugs. Among the 15 NSCLC PDXs with genetic alterations that could be established, we selected 5 PDXs generated from 4 patients and performed genomic analysis. The genetic alterations observed in clinical tests in the patients were maintained in PDXs after passaging, confirming that the PDXs inherited the driver gene alterations. When we tested the efficacy of clinically administered drugs and molecularly targeted therapies against each target, we found that some PDXs were correlated with the therapeutic effects of the patients (in the case of gefitinib and crizotinib), while others were not (in the case of lorlatinib). To elucidate this difference, the blood and intratumor drug concentrations were examined and found to be comparably low on day 21. MSI was performed to analyze the tissue structure and drug distribution in the tumor in detail. The tumor distribution could be evaluated for three of the eight drugs, and accumulation in the tumor site could be confirmed for each drug. Nevertheless, no relationship with drug efficacy could be found.

  The establishment rate of lung cancer PDXs has previously been reported to be approximately 30–50% (18,19,37,38). Several reports have associated the establishment rates with advanced stage, squamous cell carcinoma, and lack of genetic mutations (19,38,39). In our study, 55 out of 245 (22%) PDXs were established with lung cancer as a whole, and 14 out of 76 (20%) PDXs were established with genetically altered NSCLC based on clinical information (**Supplementary Table 3**). PDXs generated in tumor specimens from patients who did not receive TKIs had particularly low establishment rate percentages, and notably, no PDX was established from TKI-naïve specimens with EGFR mutation (7 implantations), ALK fusion (12 implantations), or MET skipping (one implantation). On the other hand, several PDXs could be established in tumors that became TKI-resistant. We previously analyzed the entire J-PDX library using multivariate analysis to examine factors that affected the establishment rate. Patients with a short survival time following tumor tissue collection and advanced disease demonstrate a higher establishment rate (34). In the present study, we focused on the effect of TKI treatment history in lung cancer cases and there was a higher establishment rate in TKI-resistant cases compared to that in the TKI-naive cases; however, it was not statistically significant (resistant vs naive: 25% vs 11%, p=0.15). This could be attributed to the shorter survival time in TKI-resistant cases compared to that in the TKI-naïve cases and the faster tumor growth occurring after resistance. The mechanisms of resistance after subjection to the administered molecularly targeted therapies are subdivided, considering the EGFR mutations and ALK fusion genes; the therapeutic strategies following resistance development are explored in each subpopulation. In the case of genetic abnormalities with small populations, such as ROS1 and RET fusion genes, and EGFR and ALK resistance subpopulations, it is extremely difficult to confirm the efficacy in the individual population in large-scale clinical trials. The evaluation of drug efficacy using PDX is extremely useful for such rare gene abnormalities and rare resistance mechanisms among major cancers; hence, we believe that active creation of PDX in the drug-resistant phase will be useful for

future drug development and for overcoming resistance.

We performed WES and RNA-sequencing on the five PDXs used in the study. Previous reports have shown that genetic alterations in PDXs increase copy number variations (CNVs) by passaging, but alterations that favor tumor growth, such as driver gene alterations, are retained (40). Among the PDXs analyzed in this study, the failure to confirm ALK fusion in LC-001 may be due to the specimen used for analysis. We could not confirm HER2 amplification in LC-005 by analyzing the clinical specimens and PDX tumors; however, robust HER2 expression was maintained as verified by IHC and RNA-sequencing. This suggests that HER2 positivity, in this case, is potentially caused by a mechanism other than genetic mutation or amplification. A large dataset is not available for determining the number of times a genetic analysis should be performed in PDX and for ascertaining the frequency of occurrence of genetic variations with each successive generation. In the present study, we performed genetic mutation analysis of up to three passages in five PDXs and observed that at least driver mutations were retained. However, mutations such as gene deletions and point mutations could occur through passaging. Hence, in the future, it will be necessary to comprehensively evaluate genetic changes that occur through passaging. Overall, our results showed that the driver gene alterations observed in clinical practice were generally maintained in PDXs, indicating the validity of evaluating drug efficacy in PDXs established from patients with genetic alterations.

In the drug testing of the selected five PDXs, lorlatinib resistance in clinical practice was not reproduced in LC-001 and LC-002, which was established over time before and after lorlatinib administration. On the other hand, brigatinib sensitivity was altered in these PDXs, suggesting that tumor characteristics were altered by the short lorlatinib treatment period of 2 weeks. LC-003 showed resistance to gefitinib, consistent with the clinical response. Genetic analysis showed amplification of EGFR and MET genes, which may be involved in resistance. Interestingly, osimertinib, for which EGFR and MET gene amplification has been reported as a mechanism of resistance, showed efficacy in LC-003, suggesting that it may have had some clinical efficacy (41,42). Furthermore, LC-004 was administered with crizotinib for ROS1 fusion-positive lung cancer and showed good antitumor efficacy as in clinical practice (43,44). In LC-005, pan-HER inhibitors were used to treat HER2-overexpressing PDXs, with poziotinib showing tumor reduction, while afatinib showed no efficacy. Besides, we evaluated the efficacy of T-DXd, a recently approved novel ADC for HER2, and found a dose-dependent tumor reduction (35,36). These results support the clinical efficacy of T-DXd for HER2-positive NSCLC, which was recently demonstrated in DESTINY-LUNG01 (NCT03505710) (45). In summary, our results were correlated with the clinical efficacy of certain drugs, such as gefitinib for LC-003 and crizotinib for LC-004, but also differed from clinical efficacy in other drugs, such as lorlatinib for LC-001 and LC-002.

Analysis of blood and intratumor drug concentrations was conducted to reveal factors that correlate between PDX drug efficacy and clinical response. To the best of our knowledge, this is the first report on

the evaluation of blood levels of TKIs in PDX mice. Surprisingly, both the blood and intratumor concentrations of all drugs were low at 24 h after conduction of the last drug administration. We could not find an evident association with drug efficacy; however, we confirmed that even low trough concentrations were sufficient to show efficacy in PDX mice models. We also explored the distribution of drugs in tumors and successfully visualized findings with brigatinib, crizotinib, and entrectinib. We previously analyzed the spatial distribution of various anticancer agents in tumors using MSI analysis (24-27,46-48). The spatial distribution of drugs is heterogeneous and the intra-tumor distribution of alectinib is not influenced by the expression of its target proteins (26). In the present study, crizotinib and entrectinib were homogenously distributed throughout the tissues, while brigatinib tended to be heterogeneously concentrated in the tumor site; the drug distributions were markedly not influenced by the expression of the target proteins. For other drugs, imaging using MSI was difficult, possibly due to ionization of the drug or the low effective intratumor drug concentration. The blood concentration of TKIs could be evaluated using PDX and the spatial distribution in tumors could be analyzed using MSI. No evident relationship with drug efficacy was observed; this could be attributed to the setting of the specimen collection points. To evaluate the relationship between drug efficacy and drug distribution level, it is important to understand the relationship at an optimized point over time. Analysis of the spatial distribution of drugs is useful for clarifying the mode of action of drugs. Evaluation of the differences in the distribution patterns among drugs and the effects of target protein expression or tumor stroma is helpful for drug design and for formulation of treatment strategy. We previously performed longitudinal needle biopsies at 4, 9, and 14 days after alectinib administration in a cell line transplant model and successfully assessed MSI in biopsy specimens (27). In PDX, evaluation of concentration and spatial distribution using blood and tumor samples over time will enable pharmacokinetic analysis under conditions similar to those in humans. It is necessary to evaluate systemic and intratumor pharmacology using PDX to accurately estimate the pharmacokinetics in humans.

In all five PDX models, drug efficacy was assessed to contrast the clinical responses of the four donor patients with PDX models. Four to ten mice were used in each group, and a huge variation in tumor growth rate was observed among PDXs. This may have been due to the heterogeneity of each tumor fragment. Conventionally, a 2 mm cubic tumor fragment is transplanted into a single mouse. If the tumor tissue is separated and the number of cells to be transplanted equalized, it could possibly reduce this heterogeneity. However, separation may disrupt the tumor microenvironment and result in loss of cell-cell interaction. Therefore, we transplanted the tumor "as is". Previously, Townsend et al. used acute lymphoblastic leukemia PDXs to compare the number of mice per group (between one and three) and reported that one mouse could predict the same treatment effect (49). However, in the case of solid tumors in our present study, there is more heterogeneity than in hematological tumors, encouraging the use of a larger number of mice. Our results showed a large variation in the tumor growth rate, and it would be desirable to use a large number of mice (preferably six mice per group) to evaluate the efficacy of drugs. Another important factor to consider is the location of the tumor implantation. Considering the

16 / 24

merits of tumor growth, orthotopic models in which the tumor is transplanted into the same organ of origin are desirable. However, as in lung cancer, transplantation of tumors into the body is difficult due to problems of technique and evaluation of tumor size. For this reason, we used an ectopic model as the basis of our study. However, this aspect should be examined in the future.

PDXs, in which the genetic alterations of original patients are maintained, are useful for screening drug development. Additionally, the drug exposure level differs greatly between humans and mice. Cell line-derived xenograft models are often administered at the maximum tolerated dose in mice, resulting in blood concentrations that cannot be achieved in clinical practice; the drug is often assessed to be effective *in vivo* (50). In humans, the recommended dose in the Phase I trial is set much lower than that in *in vivo* dosing due to potential adverse events with increasing doses. Whether the drug should be administered at a higher dose to match cell line-derived xenografts or rather at a lower dose to match humans in drug efficacy studies in PDXs will require further investigation.

In conclusion, we have successfully reproduced the treatment effect in patients with NSCLC PDXs with genetic alterations for some drugs. Further investigation is needed to establish appropriate evaluation methods and tools to reproduce and predict clinical outcomes with higher accuracy. We believe it is important to understand the blood concentration, intratumor concentration, and distribution in tumors using PDX.

Reference

1. Mullard A. Parsing clinical success rates. Nat Rev Drug Discov **2016**;15(7):447 doi 10.1038/nrd.2016.136.

2. Paul SM, Mytelka DS, Dunwiddie CT, Persinger CC, Munos BH, Lindborg SR*, et al.* How to improve R&D productivity: the pharmaceutical industry's grand challenge. Nat Rev Drug Discov **2010**;9(3):203-14 doi 10.1038/nrd3078.

3. Hidalgo M, Amant F, Biankin AV, Budinska E, Byrne AT, Caldas C*, et al.* Patient-derived xenograft models: an emerging platform for translational cancer research. Cancer Discov **2014**;4(9):998-1013 doi 10.1158/2159-8290.CD-14-0001.

4. Girotti MR, Lopes F, Preece N, Niculescu-Duvaz D, Zambon A, Davies L*, et al.* Paradox-breaking RAF inhibitors that also target SRC are effective in drug-resistant BRAF mutant melanoma. Cancer Cell **2015**;27(1):85-96 doi 10.1016/j.ccell.2014.11.006.

5. Bertotti A, Migliardi G, Galimi F, Sassi F, Torti D, Isella C*, et al.* A molecularly annotated platform of patient-derived xenografts ("xenopatients") identifies HER2 as an effective therapeutic target in cetuximab-resistant colorectal cancer. Cancer Discov **2011**;1(6):508-23 doi 10.1158/2159-8290.CD-11-0109.

6. Siolas D, Hannon GJ. Patient-derived tumor xenografts: transforming clinical samples into mouse models. Cancer Res **2013**;73(17):5315-9 doi 10.1158/0008-5472.CAN-13-1069.

7. Tentler JJ, Tan AC, Weekes CD, Jimeno A, Leong S, Pitts TM*, et al.* Patient-derived tumour xenografts as models for oncology drug development. Nat Rev Clin Oncol **2012**;9(6):338-50 doi 10.1038/nrclinonc.2012.61.

8. Gao H, Korn JM, Ferretti S, Monahan JE, Wang Y, Singh M*, et al.* High-throughput screening using patient-derived tumor xenografts to predict clinical trial drug response. Nat Med **2015**;21(11):1318-25 doi 10.1038/nm.3954.

9. Herbst RS, Morgensztern D, Boshoff C. The biology and management of non-small cell lung cancer. Nature **2018**;553(7689):446-54 doi 10.1038/nature25183.

10. Camidge DR, Doebele RC, Kerr KM. Comparing and contrasting predictive biomarkers for immunotherapy and targeted therapy of NSCLC. Nat Rev Clin Oncol **2019**;16(6):341-55 doi 10.1038/s41571-019-0173-9.

11. Arbour KC, Riely GJ. Systemic Therapy for Locally Advanced and Metastatic Non-Small Cell Lung Cancer: A Review. JAMA **2019**;322(8):764-74 doi 10.1001/jama.2019.11058.

12. Ettinger DS, Wood DE, Aggarwal C, Aisner DL, Akerley W, Bauman JR*, et al.* NCCN Guidelines Insights: Non-Small Cell Lung Cancer, Version 1.2020. J Natl Compr Canc Netw **2019**;17(12):1464-72 doi 10.6004/jnccn.2019.0059.

13. Duma N, Santana-Davila R, Molina JR. Non-Small Cell Lung Cancer: Epidemiology, Screening, Diagnosis, and Treatment. Mayo Clin Proc **2019**;94(8):1623-40 doi 10.1016/j.mayocp.2019.01.013.

14. Dagogo-Jack I, Shaw AT. Tumour heterogeneity and resistance to cancer therapies. Nat Rev Clin Oncol **2018**;15(2):81-94 doi 10.1038/nrclinonc.2017.166.

15.   Gerlinger M. Targeted drugs ramp up cancer mutability. Science **2019**;366(6472):1452-3 doi 10.1126/science.aaz9900.

16.   Billingham L, Malottki K, Steven N. Research methods to change clinical practice for patients with rare cancers. The Lancet Oncology **2016**;17(2):e70-e80 doi 10.1016/s1470-2045(15)00396-4.

17.   Jiang Y, Zhao J, Zhang Y, Li K, Li T, Chen X, *et al.* Establishment of lung cancer patient-derived xenograft models and primary cell lines for lung cancer study. J Transl Med **2018**;16(1):138 doi 10.1186/s12967-018-1516-5.

18.   Kang HN, Choi JW, Shim HS, Kim J, Kim DJ, Lee CY, *et al.* Establishment of a platform of non-small-cell lung cancer patient-derived xenografts with clinical and genomic annotation. Lung Cancer **2018**;124:168-78 doi 10.1016/j.lungcan.2018.08.008.

19.   Kita K, Fukuda K, Takahashi H, Tanimoto A, Nishiyama A, Arai S, *et al.* Patient-derived xenograft models of non-small cell lung cancer for evaluating targeted drug sensitivity and resistance. Cancer Sci **2019**;110(10):3215-24 doi 10.1111/cas.14171.

20.   Morgan KM, Riedlinger GM, Rosenfeld J, Ganesan S, Pine SR. Patient-Derived Xenograft Models of Non-Small Cell Lung Cancer and Their Potential Utility in Personalized Medicine. Front Oncol **2017**;7:2 doi 10.3389/fonc.2017.00002.

21.   Nakajima T, Geddie W, Anayama T, Ko HM, da Cunha Santos G, Boerner S, *et al.* Patient-derived tumor xenograft models established from samples obtained by endobronchial ultrasound-guided transbronchial needle aspiration. Lung Cancer **2015**;89(2):110-4 doi 10.1016/j.lungcan.2015.05.018.

22.   Zhang F, Wang W, Long Y, Liu H, Cheng J, Guo L, *et al.* Characterization of drug responses of mini patient-derived xenografts in mice for predicting cancer patient clinical therapeutic response. Cancer Commun (Lond) **2018**;38(1):60 doi 10.1186/s40880-018-0329-5.

23.   Kim HR, Kang HN, Shim HS, Kim EY, Kim J, Kim DJ, *et al.* Co-clinical trials demonstrate predictive biomarkers for dovitinib, an FGFR inhibitor, in lung squamous cell carcinoma. Ann Oncol **2017**;28(6):1250-9 doi 10.1093/annonc/mdx098.

24.   Nishidate M, Hayashi M, Aikawa H, Tanaka K, Nakada N, Miura SI, *et al.* Applications of MALDI mass spectrometry imaging for pharmacokinetic studies during drug development. Drug Metab Pharmacokinet **2019**;34(4):209-16 doi 10.1016/j.dmpk.2019.04.006.

25.   Nishimura M, Hayashi M, Mizutani Y, Takenaka K, Imamura Y, Chayahara N, *et al.* Distribution of erlotinib in rash and normal skin in cancer patients receiving erlotinib visualized by matrix assisted laser desorption/ionization mass spectrometry imaging. Oncotarget **2018**;9(26):18540-7 doi 10.18632/oncotarget.24928.

26.   Ryu S, Hayashi M, Aikawa H, Okamoto I, Fujiwara Y, Hamada A. Heterogeneous distribution of alectinib in neuroblastoma xenografts revealed by matrix-assisted laser desorption ionization mass spectrometry imaging: a pilot study. Br J Pharmacol **2018**;175(1):29-37 doi 10.1111/bph.14067.

27.   Ryu S, Ohuchi M, Yagishita S, Shimoi T, Yonemori K, Tamura K, *et al.* Visualization of the distribution of nanoparticle-formulated AZD2811 in mouse tumor model using matrix-assisted laser desorption ionization mass spectrometry imaging. Sci Rep **2020**;10(1):15535 doi 10.1038/s41598-020-72665-5.

28. Cross DA, Ashton SE, Ghiorghiu S, Eberlein C, Nebhan CA, Spitzler PJ, *et al.* AZD9291, an irreversible EGFR TKI, overcomes T790M-mediated resistance to EGFR inhibitors in lung cancer. Cancer Discov **2014**;4(9):1046-61 doi 10.1158/2159-8290.CD-14-0337.

29. Zhang S, Anjum R, Squillace R, Nadworny S, Zhou T, Keats J, *et al.* The Potent ALK Inhibitor Brigatinib (AP26113) Overcomes Mechanisms of Resistance to First- and Second-Generation ALK Inhibitors in Preclinical Models. Clin Cancer Res **2016**;22(22):5527-38 doi 10.1158/1078-0432.CCR-16-0569.

30. Robichaux JP, Elamin YY, Tan Z, Carter BW, Zhang S, Liu S, *et al.* Mechanisms and clinical activity of an EGFR and HER2 exon 20-selective kinase inhibitor in non-small cell lung cancer. Nat Med **2018**;24(5):638-46 doi 10.1038/s41591-018-0007-9.

31. Yun MR, Kim DH, Kim SY, Joo HS, Lee YW, Choi HM, *et al.* Repotrectinib Exhibits Potent Antitumor Activity in Treatment-Naive and Solvent-Front-Mutant ROS1-Rearranged Non-Small Cell Lung Cancer. Clin Cancer Res **2020**;26(13):3287-95 doi 10.1158/1078-0432.CCR-19-2777.

32. Ardini E, Menichincheri M, Banfi P, Bosotti R, De Ponti C, Pulci R, *et al.* Entrectinib, a Pan-TRK, ROS1, and ALK Inhibitor with Activity in Multiple Molecularly Defined Cancer Indications. Mol Cancer Ther **2016**;15(4):628-39 doi 10.1158/1535-7163.MCT-15-0758.

33. Yoon S, Xuan Z, Makarov V, Ye K, Sebat J. Sensitive and accurate detection of copy number variants using read depth of coverage. Genome Res **2009**;19(9):1586-92 doi 10.1101/gr.092981.109.

34. Yagishita S, Kato K, Takahashi M, Imai T, Yatabe Y, Kuwata T, *et al.* Characterization of the large-scale Japanese patient-derived xenograft (J-PDX) library. Cancer Sci **2021** doi 10.1111/cas.14899.

35. Shitara K, Bang YJ, Iwasa S, Sugimoto N, Ryu MH, Sakai D, *et al.* Trastuzumab Deruxtecan in Previously Treated HER2-Positive Gastric Cancer. N Engl J Med **2020**;382(25):2419-30 doi 10.1056/NEJMoa2004413.

36. Modi S, Saura C, Yamashita T, Park YH, Kim SB, Tamura K, *et al.* Trastuzumab Deruxtecan in Previously Treated HER2-Positive Breast Cancer. N Engl J Med **2020**;382(7):610-21 doi 10.1056/NEJMoa1914510.

37. Izumchenko E, Paz K, Ciznadija D, Sloma I, Katz A, Vasquez-Dunddel D, *et al.* Patient-derived xenografts effectively capture responses to oncology therapy in a heterogeneous cohort of patients with solid tumors. Ann Oncol **2017**;28(10):2595-605 doi 10.1093/annonc/mdx416.

38. John T, Kohler D, Pintilie M, Yanagawa N, Pham NA, Li M, *et al.* The ability to form primary tumor xenografts is predictive of increased risk of disease recurrence in early-stage non-small cell lung cancer. Clin Cancer Res **2011**;17(1):134-41 doi 10.1158/1078-0432.CCR-10-2224.

39. Stewart EL, Mascaux C, Pham NA, Sakashita S, Sykes J, Kim L, *et al.* Clinical Utility of Patient-Derived Xenografts to Determine Biomarkers of Prognosis and Map Resistance Pathways in EGFR-Mutant Lung Adenocarcinoma. J Clin Oncol **2015**;33(22):2472-80 doi 10.1200/JCO.2014.60.1492.

40. Ben-David U, Ha G, Tseng YY, Greenwald NF, Oh C, Shih J, *et al.* Patient-derived xenografts undergo mouse-specific tumor evolution. Nat Genet **2017**;49(11):1567-75 doi 10.1038/ng.3967.

41. Nakatani K, Yamaoka T, Ohba M, Fujita KI, Arata S, Kusumoto S, *et al.* KRAS and EGFR Amplifications Mediate Resistance to Rociletinib and Osimertinib in Acquired Afatinib-Resistant

NSCLC Harboring Exon 19 Deletion/T790M in EGFR. Mol Cancer Ther **2019**;18(1):112-26 doi 10.1158/1535-7163.Mct-18-0591.

42.   Leonetti A, Sharma S, Minari R, Perego P, Giovannetti E, Tiseo M. Resistance mechanisms to osimertinib in EGFR-mutated non-small cell lung cancer. Br J Cancer **2019**;121(9):725-37 doi 10.1038/s41416-019-0573-8.

43.   Shaw AT, Riely GJ, Bang YJ, Kim DW, Camidge DR, Solomon BJ*, et al.* Crizotinib in ROS1-rearranged advanced non-small-cell lung cancer (NSCLC): updated results, including overall survival, from PROFILE 1001. Ann Oncol **2019**;30(7):1121-6 doi 10.1093/annonc/mdz131.

44.   Shaw AT, Ou SH, Bang YJ, Camidge DR, Solomon BJ, Salgia R*, et al.* Crizotinib in ROS1-rearranged non-small-cell lung cancer. N Engl J Med **2014**;371(21):1963-71 doi 10.1056/NEJMoa1406766.

45.   Smit EF, Nakagawa K, Nagasaka M, Felip E, Goto Y, Li BT*, et al.* Trastuzumab deruxtecan (T-DXd; DS-8201) in patients with HER2-mutated metastatic non-small cell lung cancer (NSCLC): Interim results of DESTINY-Lung01. Journal of Clinical Oncology **2020**;38(15_suppl):9504- doi 10.1200/JCO.2020.38.15_suppl.9504.

46.   Hayashi Y, Ohuchi M, Ryu S, Yagishita S, Hamada A. A procedure for method development and protein binding ratio as the indicator of sensitivity with anticancer agents on MALDI mass spectrometry imaging. Drug Metab Pharmacokinet **2021**;38:100385 doi 10.1016/j.dmpk.2021.100385.

47.   Nishidate M, Yamamoto K, Masuda C, Aikawa H, Hayashi M, Kawanishi T*, et al.* MALDI mass spectrometry imaging of erlotinib administered in combination with bevacizumab in xenograft mice bearing B901L, EGFR-mutated NSCLC cells. Sci Rep **2017**;7(1):16763 doi 10.1038/s41598-017-17211-6.

48.   Tsubata Y, Hayashi M, Tanino R, Aikawa H, Ohuchi M, Tamura K*, et al.* Evaluation of the heterogeneous tissue distribution of erlotinib in lung cancer using matrix-assisted laser desorption ionization mass spectrometry imaging. Sci Rep **2017**;7(1):12622 doi 10.1038/s41598-017-13025-8.

49.   Townsend EC, Murakami MA, Christodoulou A, Christie AL, Koster J, DeSouza TA*, et al.* The Public Repository of Xenografts Enables Discovery and Randomized Phase II-like Trials in Mice. Cancer Cell **2016**;29(4):574-86 doi 10.1016/j.ccell.2016.03.008.

50.   Thompson J, Stewart CF, Houghton PJ. Animal models for studying the action of topoisomerase I targeted drugs. Biochim Biophys Acta **1998**;1400(1-3):301-19 doi 10.1016/s0167-4781(98)00143-2.

Table 1. Patient characteristics

Patient	Age	Sex	Histology	Clinical driver gene	TNM Staging	Smoking Status	Treatment	PDX No.	PDX sample (Collection point)	Pt sequence sample (Collection point)	Gene alteration
A	70	F	Adeno	EML4-ALK (IHC)	T2aN3M1a IV	Never	1st line: alectinib 2nd line: CBDCA+PEM 3rd line: ceritinib	LC-001	Pleural effusion (Before 5th line)	Pleural effusion (Before 5th line)	Pt: MDM2 amp (CN=19.6) TG1: EML4-ALK, MDM2 amp (CN=23.7) TG2: MDM2 amp (CN=21.7) TG3: EML4-ALK, MDM2 amp (CN=23.2)
							4th line: TS-1 5th line: lorlatinib 6th line: alectinib	LC-002	Pleural effusion (After 5th line)	Pleural effusion (Before 5th line)	Pt: MDM2 amp (CN=19.6) TG1: EML4-ALK, MDM2 amp (CN=22.8) TG2: EML4-ALK, MDM2 amp (CN=19.8) TG3: EML4-ALK, MDM2 amp (CN=20.6)
B	42	F	Adeno	EGFR ex21 L858R (Dako)	T3N3M0 IIIB	Never	1st line: gefitinib 2nd line: clinical trial	LC-003	Bronchoscopic specimen (After 2nd line)	FFPE (Time of Diagnosis)	Pt: EGFR ex21 L858R (29.5%) TG1: EGFR ex21 L858R (53.9%), EGFR amp (CN=6.6), MET amp (CN=6.0) TG2: EGFR ex21 L858R (50.2%), EGFR amp (CN=6.3), MET amp (CN=6.1) TG3: EGFR ex21 L858R (51.8%), EGFR amp (CN=6.1), MET amp (CN=4.9)
C	46	M	Adeno	EZR-ROS1 (RT-PCR)	TxN3M1a IVa	Former	1st line: CDDP+PEM 2nd line: nivolumab 3rd line: TS-1 4th line: crizotinib	LC-004	Pleural effusion (After 3rd line)	FFPE (Time of Diagnosis)	Pt: PIK3CA (21.6%) TG1: EZR-ROS1, PIK3CA (100%)
D	59	M	Adeno	HER2 Amplification (OCA)	T2bN2M1a IVa	Never	1st line: CBDCA+nab-PTX 2nd line: atezolizumab 3rd line: nivolumab 4th line: TS-1	LC-005	Pleural effusion (After 2nd line)	Pleural effusion (After 2nd line)	Pt: TP53 (33.4%), SMARCA4 (43.8%) TG1: TP53 (100%), SMARCA4 (100%) TG2: TP53 (100%), SMARCA4 (100%)

Abbreviations: F, female; M, male; TNM, tumor-node-metastasis; ALK, anaplastic lymphoma kinase; EGFR, epidermal growth factor receptor; HER2, human epidermal growth factor receptor type 2; ROS1, c-ros oncogene 1; IHC, Immunohistochemistry; Dako, Dako EGFR pharmDx; OCA, Oncomine Comprehensive Assay ver3; RT-PCR, real-time polymerase chain reaction; CBDCA, carboplatin; PEM, pemetrexed; nab-PTX, nab-paclitaxel; CDDP, cisplatin Pt, patient.

Table 2. Drug concentration in PDX-mice plasma and tumor samples.

PDX No.	Drug	Tumor (mean ± SD, ng/mg)	Plasma (mean ± SD, ng/mL)
LC-001	Brigatinib	25 ± 6.2	5.5 ± 1.0
	Lorlatinib	6.2 ± 4.0	39 ± 25
LC-002	Brigatinib	40 ± 27	5.6 ± 2.9
	Lorlatinib	2.4 ± 0.8	18 ± 5.7
LC-003	Osimertinib	3.7 ± 1.6	<2
	Gefitinib	2.1 ± 0.8	<2
LC-004	Crizotinib	253 ± 119	43 ± 33
	Entrectinib	156 ± 124	55 ± 19
LC-005	Afatinib	ND	ND
	Poziotinib	ND	1.2 ± 0.6

Abbreviations: PDX, Patient-derived xenograft; ND, Not detectable; SD, standard deviation.

Figure legends

Figure 1. CONSORT diagram and study design

The selection criteria for PDX used in this study are shown in Figure 1A. Of the 55-lung cancer PDXs, 47 were non-small cell lung cancer PDXs, and 15 were driver gene positive. In this study, we used 5 of these PDXs. Five driver gene positive PDXs were used to evaluate the efficacy of molecularly targeted agents and to analyze blood concentration, intratumor concentration, and intratumor drug distribution (Figure 1B).

Figure 2. Histological findings of patient tissue and PDX tissue

Hematoxylin and eosin (H&E) staining of patient tissue and PDX (TG1-3) tissue. Overall, the original morphology was maintained after establishment and passage of PDXs, but increased malignancy was observed in some PDXs. The H&E staining of Patient A's specimen at diagnosis is shown as the patient tumor in LC-001 and LC-002. X20.

Figure 3. Evaluation of the drug treatment in vivo

The treatment course of the original patient in each PDX, the time of PDX specimen collection, and the results of PDX drug efficacy studies are shown. The upper band shows the chemotherapy regimen, best response, and PFS (month). Figure 3A shows LC-001 and 002 generated from Patient A (ALK fusion), Figure 3B shows LC-003 generated from Patient B (EGFR mutation), Figure 3C shows LC-004 generated from Patient C (ROS1 fusion), and Figure 3D shows LC-005 generated from Patient D (HER2 amplification). N means the number of mice used in each group. P value indicates Dunnett's multiple comparison adjusted P value comparing between control and each group at day 21 after two-way ANOVA. BW (%) indicates percent bodyweight change in each group at day 0 and day 21. Error bars represent the mean ± SEM.

Figure 4. Mass spectrometry imaging

Figure 4A: H&E staining, immunostaining of target proteins, and MSI images of PDX tumor tissues treated with each drug.

Figure 3B: Comparison of drug intensities at tumor and non-tumor sites in the H&E images. Brigatinib shows accumulation at tumor sites, whereas crizotinib and entrectinib show overall accumulation.

Figure 1. CONSORT diagram and study design

Figure 1A. CONSORT diagram
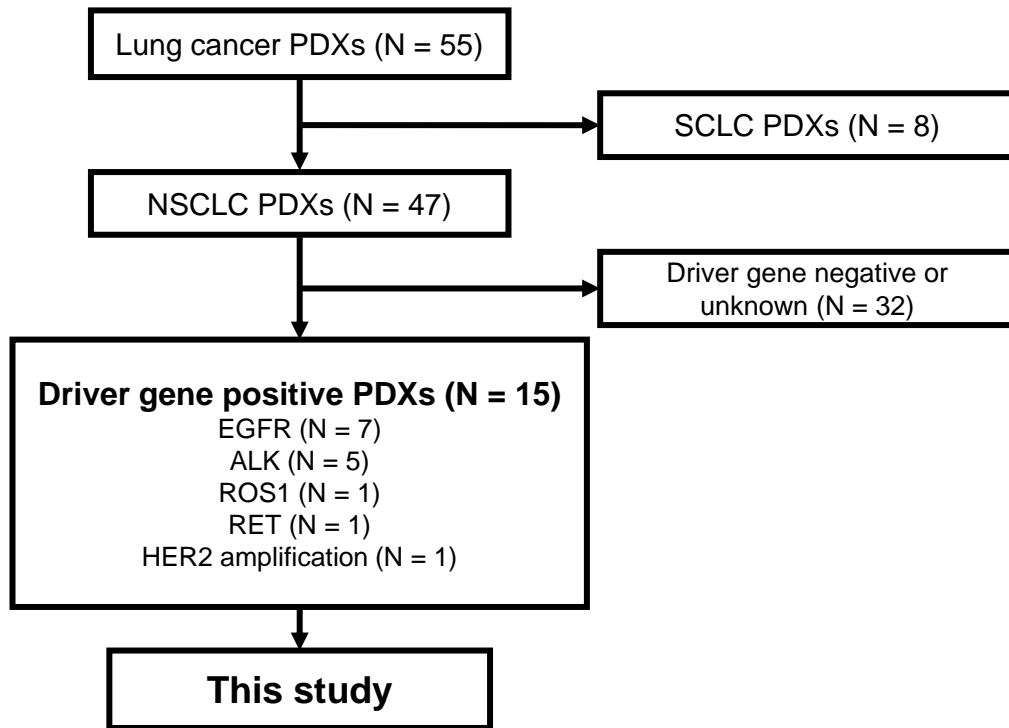
Abbreviations: NSCLC, non-small cell lung cancer; SCLC, small cell lung cancer; EGFR, epidermal growth factor receptor; ALK, anaplastic lymphoma kinase; ROS1, c-ros oncogene 1; RET, rearranged during transfection; HER2, human epidermal growth factor receptor type 2.
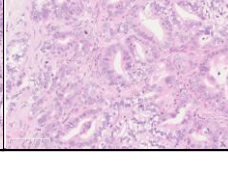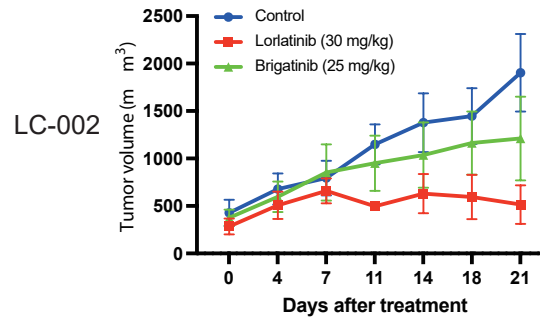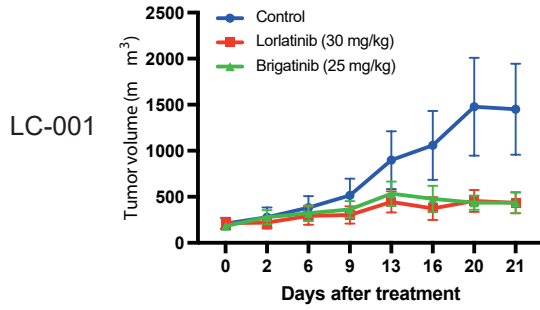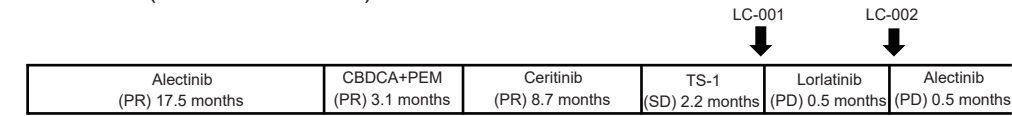
Figure 1B. Study design
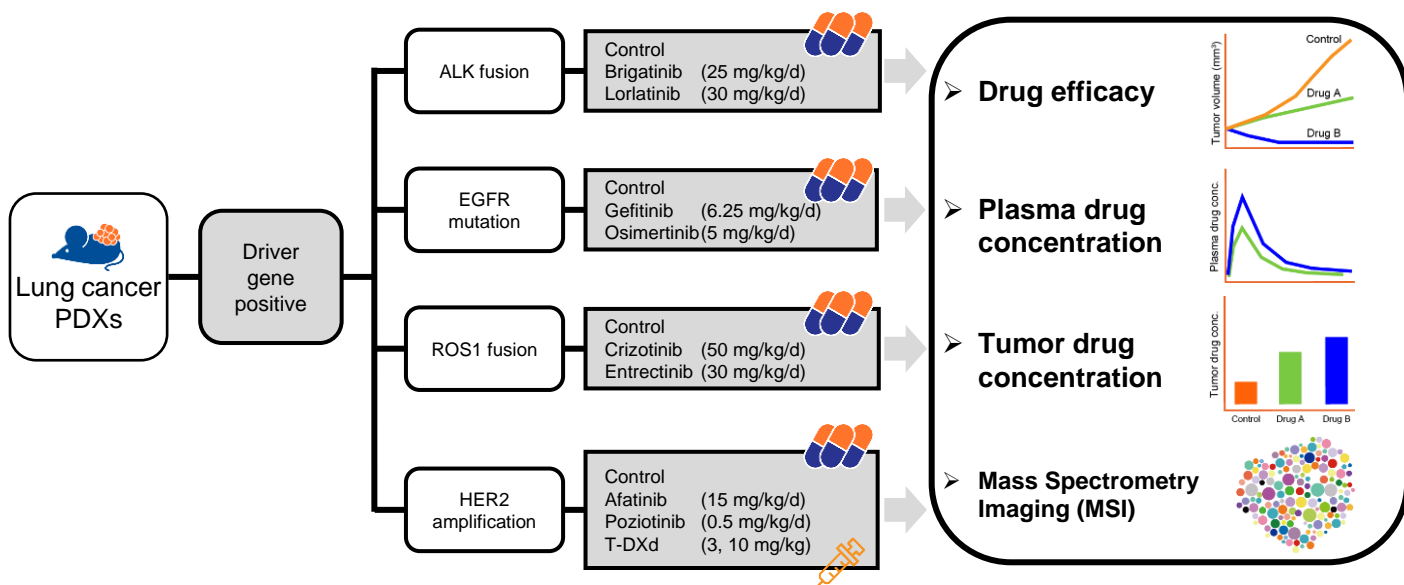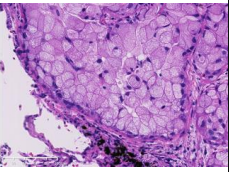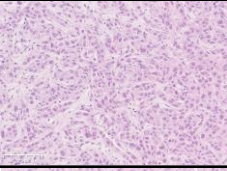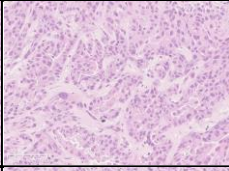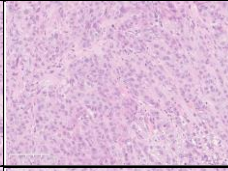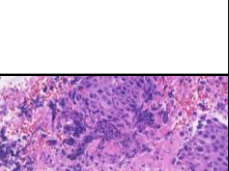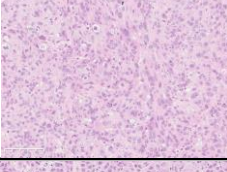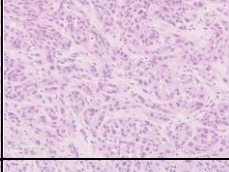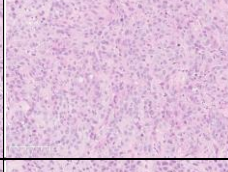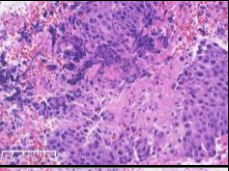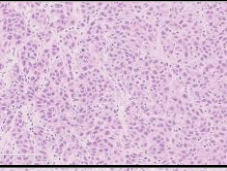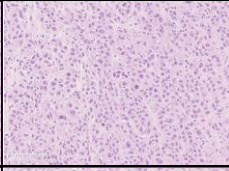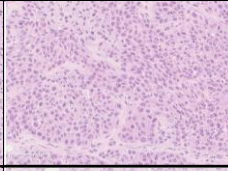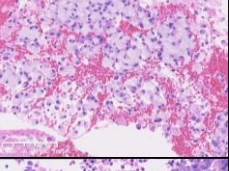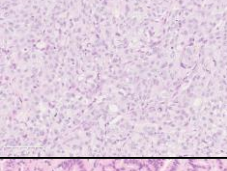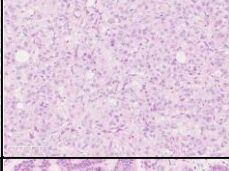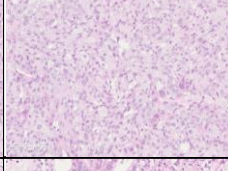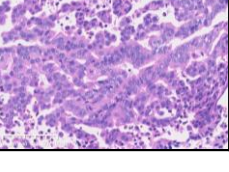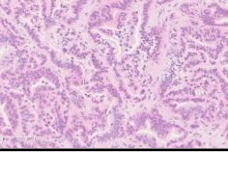
Figure 2. Histological findings of patient tissue and PDX tissue

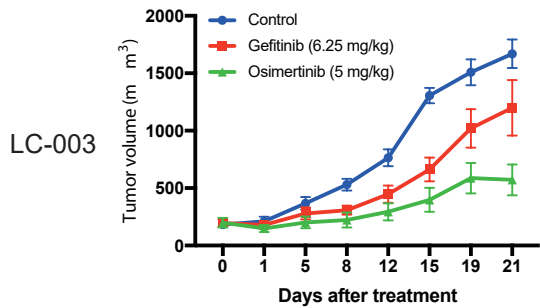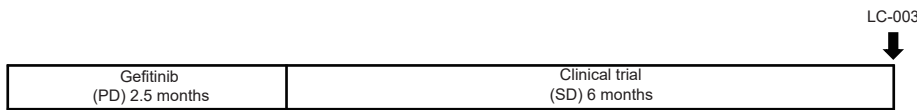| Patient No.	PDX No.	Patient	TG1	TG2	TG3
A	LC-001				
	LC-002				
B	LC-003				
C	LC-004				
D	LC-005				

Abbreviation: TG, trans generation.
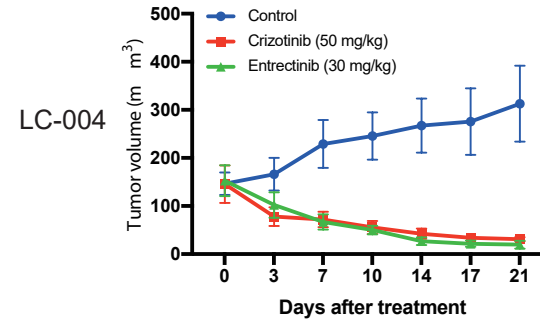
Figure 3. Evaluation of the drug treatment in vivo

A. Patient A (EML4-ALK fusion)

LC-001 ↓ LC-002 ↓

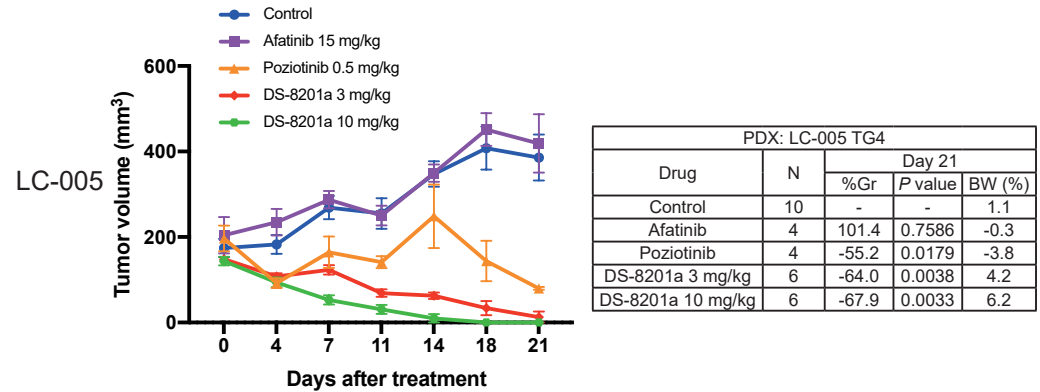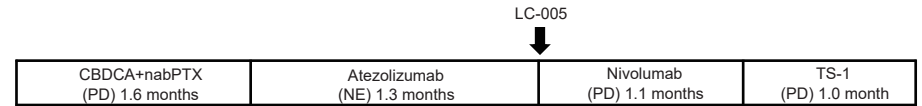| Alectinib (PR) 17.5 months	CBDCA+PEM (PR) 3.1 months	Ceritinib (PR) 8.7 months	TS-1 (SD) 2.2 months	Lorlatinib (PD) 0.5 months	Alectinib (PD) 0.5 months

LC-001

Tumor volume (mm³) vs Days after treatment (0, 2, 6, 9, 13, 16, 20, 21)
- Control
- Lorlatinib (30 mg/kg)
- Brigatinib (25 mg/kg)

PDX: LC-001 TG4				
Drug	N	Day 21		
		%Gr	P value	BW (%)
Control	4	-	-	7.0
Lorlatinib	4	17.8	0.0790	8.2
Brigatinib	4	20.5	0.0790	3.0

LC-002

Tumor volume (mm³) vs Days after treatment (0, 4, 7, 11, 14, 18, 21)
- Control
- Lorlatinib (30 mg/kg)
- Brigatinib (25 mg/kg)

PDX: LC-002 TG4				
Drug	N	Day 21		
		%Gr	P value	BW (%)
Control	4	-	-	-4.9
Lorlatinib	4	15.6	0.7625	0.2
Brigatinib	4	56.6	0.1318	6.7

B. Patient B (EGFR ex21 L858R with EGFR and MET amplification)

LC-003 ↓

Gefitinib (PD) 2.5 months	Clinical trial (SD) 6 months

LC-003

Tumor volume (mm³) vs Days after treatment (0, 1, 5, 8, 12, 15, 19, 21)
- Control
- Gefitinib (6.25 mg/kg)
- Osimertinib (5 mg/kg)

PDX: LC-003 TG4				
Drug	N	Day 21		
		%Gr	P value	BW (%)
Control	4	-	-	7.9
Gefitinib	4	67.5	0.1590	2.4
Osimertinib	4	25.1	0.0017	4.6

C. Patient C (EZR-ROS1 fusion)

LC-004 ↓

CDDP+PEM (PR) 11.9 months	Nivolumab (NE) 1.1 months	TS-1 (SD) 14.9 months	Crizotinib (NE) 0.6 months

LC-004

Tumor volume (mm³) vs Days after treatment (0, 3, 7, 10, 14, 17, 21)
- Control
- Crizotinib (50 mg/kg)
- Entrectinib (30 mg/kg)

PDX: LC-004 TG3				
Drug	N	Day 21		
		%Gr	P value	BW (%)
Control	5	-	-	-2.3
Crizotinib	4	-68.8	0.0272	-2.1
Entrectinib	5	-80.0	0.0169	0.3

D. Patient D (HER2 amplification)

LC-005 ↓

CBDCA+nabPTX (PD) 1.6 months	Atezolizumab (NE) 1.3 months	Nivolumab (PD) 1.1 months	TS-1 (PD) 1.0 month

LC-005

Tumor volume (mm³) vs Days after treatment (0, 4, 7, 11, 14, 18, 21)
- Control
- Afatinib 15 mg/kg
- Poziotinib 0.5 mg/kg
- DS-8201a 3 mg/kg
- DS-8201a 10 mg/kg

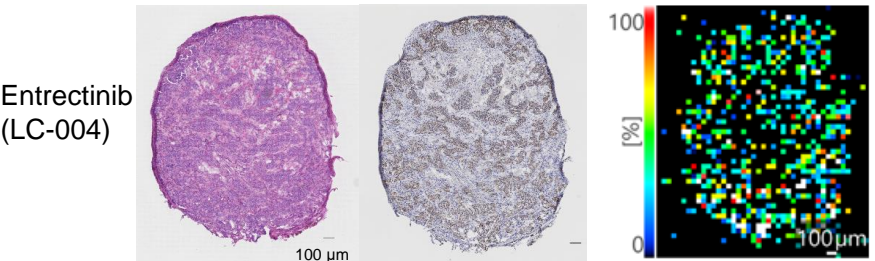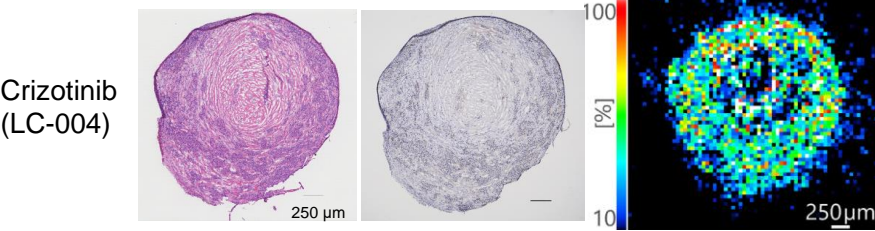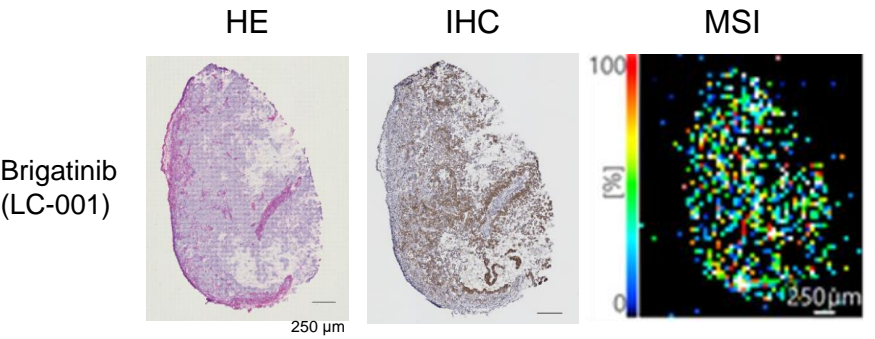| PDX: LC-005 TG4				
Drug	N	Day 21		
		%Gr	P value	BW (%)
Control	10	-	-	1.1
Afatinib	4	101.4	0.7586	-0.3
Poziotinib	4	-55.2	0.0179	-3.8
DS-8201a 3 mg/kg	6	-64.0	0.0038	4.2
DS-8201a 10 mg/kg	6	-67.9	0.0033	6.2

Abbreviations: CBDCA, Carboplatin; PEM, Pemetrexed; CDDP, Cisplatin; nabPTX, Albumin-bound formulation paclitaxel; PR, Partial response; SD, Stable disease; PD, Progressive disease; NE, Not evaluable.
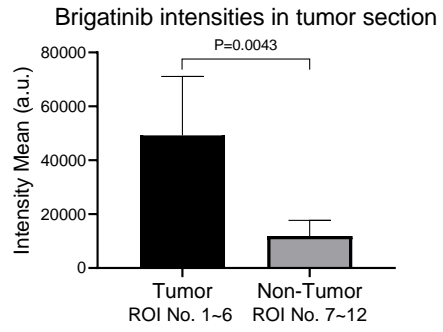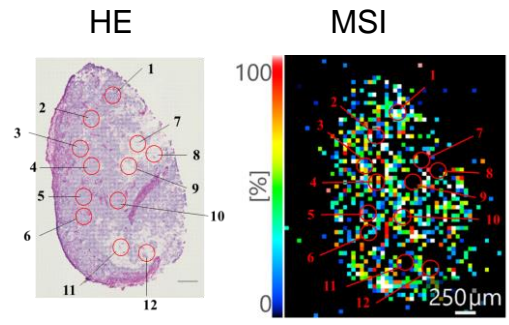
Figure 4. Mass spectrometry imaging
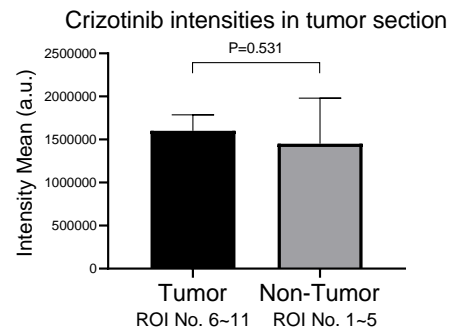
A. Mass Spectrometry Imaging of the drug distribution.

B. Region of interest analysis